Nanometric multiscale rough Zn–ZnO superhydrophobic thin films: Self-diffusion of zinc and effect of UV irradiation

Harish C. Barshilia,[a] K. R. Sai Tej, L. Mayura Devi, and K. S. Rajam
Surface Engineering Division, National Aerospace Laboratories (CSIR), Bangalore 560017, India

(Received 12 July 2010; accepted 4 August 2010; published online 14 October 2010)

Zn–ZnO superhydrophobic thin films have been prepared by thermal oxidation of sputtered Zn. The superhydrophobicity observed in these coatings is attributed to multiscale roughness in the nanometric range only. The higher scale roughness was due to the combination of nanoclusters (solid regions) and air gaps while the lower scale roughness was due to the textured surface created by the fusion of individual ZnO nanocrystals to form the nanoclusters. The superhydrophobicity in these coatings has been observed only for an optimum combination of solid regions (i.e., nanoclusters) and air pockets. Experimental evidences have been provided to demonstrate that an additional micron-scale roughness on the substrate does not affect the wettability of the coating. It has been observed that the wettability of the Zn–ZnO coatings changes from hydrophobic to superhydrophobic during the initial 24 h after deposition. This occurs due to the outward self-diffusion of Zn to the surface and its subsequent oxidation under ambient conditions. Field-emission scanning electron microscopy (FESEM) and atomic force microscopy (AFM) were used to demonstrate the morphological changes while micro-Raman spectroscopy was used to record the chemical changes on the coating surface as a result of the outward diffusion and subsequent oxidation of Zn. Studies have also been carried out to determine the effect of UV irradiation on the Zn–ZnO coatings. The UV irradiation transformed the Zn–ZnO surface from superhydrophobic to hydrophilic. Our studies based on FESEM, AFM, micro-Raman spectroscopy, and roughness profilometry show that this transformation was mainly due to the morphological changes that occur in addition to the chemical changes taking place on the ZnO surface under the influence of UV irradiation. The UV irradiation disturbs the optimum density of air pockets, leading to the loss of superhydrophobicity. © *2010 American Institute of Physics*. [doi:10.1063/1.3487925]

I. INTRODUCTION

Solid surfaces can be divided into two categories based on the wettability of water on that surface—hydrophilic and hydrophobic, i.e., surfaces with contact angle (CA) $<90°$ and surfaces with CA $>90°$. A hydrophobic surface with a CA greater than 150° is termed as a superhydrophobic surface. Naturally occurring superhydrophobic surfaces are observed on the leaves of some plants and on the wings and limbs of certain insects.[1,2] The superhydrophobic nature of these surfaces has been attributed to the combination of micrometer and nanometer scale roughness and the presence of low surface energy materials or nanostructured surfaces.[1–4] Over the years, there have been many attempts to replicate the superhydrophobic behavior observed in nature and various methods have been reported to prepare the same.[5–8] Other properties such as color, transparency, breathability, reversibility, etc. have also been integrated into superhydrophobic surfaces. Superhydrophobic surfaces have a wide variety of applications such as antibiofouling coatings,[9,10] anticing, and antisticking of snow,[11] humidity proof coatings on glass and metals,[12] optical coatings,[13] drag reduction, water and bacteria proof upholstery, etc.

Zinc oxide (ZnO) is a wide band gap II–VI semiconductor with a band gap of 3.3 eV, which crystallizes in the hexagonal-wurtzite crystal structure. ZnO finds important uses in electronics, UV detectors, chemical and biological sensors, solar cells, piezoelectric materials, and as catalysts. ZnO is also extremely important in its nanostructured form. ZnO has been deposited in the nanostructured form as nanoneedles, nanonails, nanoclusters, nanorod arrays, etc. Recently, there has been a lot of interest in the superhydrophobic properties of nanostructured ZnO.[14,15] The addition of superhydrophobic properties in addition to those listed above opens up an array of potential uses for ZnO. Wettability switching of ZnO nanostructures from superhydrophobic to superhydrophilic state under the influence of UV irradiation has also been reported.[14,16]

Earlier reports suggested the necessity of dual microscale and nanoscale roughness of a given surface to exhibit superhydrophobic properties.[17,18] Here, we report the preparation of a nanometric multiscale rough Zn–ZnO superhydrophobic coating. Zn–ZnO coatings were prepared by thermal oxidation of Zn at a temperature in the range of 250–325 °C in a sputtering chamber for 2 h. This resulted in the formation of a thin ZnO layer on the Zn surface. The Zn–ZnO coating consisted of nanoclusterlike microstructure interspersed with air pockets. The nanoclusters were formed by the fusion of individual rodlike structures which gave rise to a patterned or textured surface. These nanoclusters and fused nanorodlike structures gave rise to different scales of nanometric roughness in the coating, which was responsible for

[a]Electronic mail: harish@nal.res.in.

 © 2010 American Institute of Physics

Author complimentary copy. Redistribution subject to AIP license or copyright, see http://jap.aip.org/jap/copyright.jsp

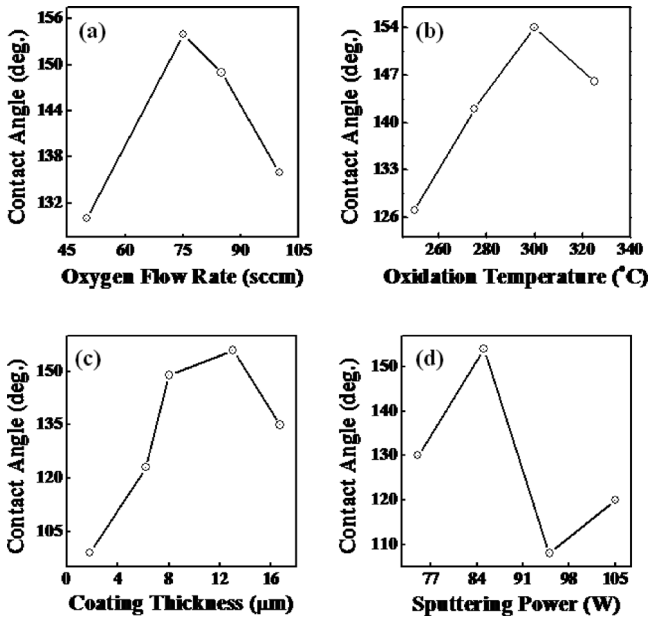

FIG. 1. Variations in water CA with: (a) Oxygen flow rate, (b) oxidation temperature, (c) coating thickness, and (d) sputtering power.

the superhydrophobic behavior. Experimental evidences have been provided to show that the introduction of an additional micron-scale roughness does not change the wettability of such a Zn–ZnO coating. It is well known that ZnO is a stable material, however, Zn–ZnO is not as stable due to the self-diffusion of Zn that occurs even at room temperature.[19] The outward self-diffusion of Zn in Zn–ZnO is expected to affect the microstructure and subsequently the wettability, which to our knowledge has not been studied. In the present work, it was observed that Zn–ZnO coating achieved superhydrophobicity 24 h after deposition. During this time, it was left in ambient conditions. Experimental observations supporting the process of outward self-diffusion of Zn and its effect on the wettability have been recorded using field-emission scanning electron microscopy (FESEM), micro-Raman spectroscopy, atomic force microscopy (AFM), and CA goniometer.

In addition to the preparation of the superhydrophobic surface, we also investigated the effect of ultraviolet (UV) irradiation on the Zn–ZnO coating. Previous reports on switching wettability of ZnO thin films have explained the mechanism based on hydroxyl adsorption onto oxygen vacancies created via a reaction with holes generated as electron–hole pairs during UV irradiation.[14,16] As far as we know, there have been no reports on the structural and morphological changes that occur in Zn–ZnO coatings as a result of UV irradiation. This paper details the observed morphological changes in the coatings due to UV exposure. Our studies based on FESEM, micro-Raman spectroscopy, and AFM suggest that the switching is also a result of the photoinduced surface morphological changes. A possible mechanism to account for the switching is discussed based on the morphological changes.

II. EXPERIMENTAL DETAILS

Zn–ZnO nanoclustered coatings were deposited on glass and silicon substrates in a radio frequency (f=13.56 MHz) balanced magnetron sputtering system. The target used was a 0.075 m diameter and 0.006 m thick zinc disk (99.99% purity). The distance between the target and the substrates was 0.054 m. The substrates were cleaned using isopropyl alcohol and acetone in an ultrasonic agitator prior to the deposition process. The samples were loaded in the deposition chamber and the chamber was pumped down to 6.0×10^{-4} Pa before the deposition process. Argon (99.99%) was let into the system at a flow rate of 25 SCCM (SCCM denotes cubic centimeter per minute at STP) and the target was cleaned using argon plasma for 5 min prior to the deposition. Zinc was deposited on the substrates at different values of target power (75–100 W) and sputtering time (3–15 min). The zinc deposition was carried out at a substrate temperature of 200 °C. Post zinc deposition, thermal oxidation of the samples was carried out. The temperature during the oxidation process was varied from 250–325 °C. The flow rate of oxygen was varied between 50 and 100 SCCM. The oxidation process was carried out for a period of 2 h. The thickness of Zn–ZnO coating was varied between 2 and 17 μm.

The x-ray diffraction (XRD) patterns of the coatings were recorded in a Rigaku D/max 2200 Ultima x-ray powder diffractometer with thin film attachment (α=3°). The x-ray source was a Cu K_α radiation (λ=0.15418 nm), which was operated at 40 kV and 30 mA. The bonding structure of the coatings was characterized by x-ray photoelectron spectroscopy (XPS) using an ESCA 3000 (V.G. Microtech) system with a monochromatic Al K_α x-ray beam (energy =1486.5 eV and power=150 W). The chemical structure of the coatings was measured using micro-Raman spectroscopy. A DILOR-Jobin-Yvon-SPEX integrated micro-Raman spectrometer was used for the present study. Three-dimensional surface imaging of the coatings was measured using AFM (Surface Imaging Systems). The average surface roughness (R_a) of the ZnO coatings was measured using Mitutoyo surface roughness tester (SURFTEST 301). The microstructure of the coatings was studied using FESEM (Supra 40 VP, Carl Zeiss). The static CA was measured according to the sessile drop method using a CA analyzer (Phoenix 300 goniometer) with deionized water. The system mainly consists of a CCD video camera with a resolution of 768×576 pixels. The drop image was stored by the video camera and an image analysis system calculated both the left and right angles from the shape of the drop with an accuracy of ±0.1°. The droplet size of the fluid was about 5 μl, therefore, the gravitational effects can be neglected. The CA of the samples was measured at three places and the values reported herein are the averages of three measurements. A UV lamp of 200 W was used to study the effect of UV irradiation on the properties of Zn–ZnO coatings.

III. RESULTS AND DISCUSSION

A. Optimization of process parameters

The process parameters were optimized as a function of the CA. The parameters optimized were: the flow rate of oxygen, the oxidation temperature, the coating thickness and the target power. Variations in CA with oxygen flow rate,

Author complimentary copy. Redistribution subject to AIP license or copyright, see http://jap.aip.org/jap/copyright.jsp

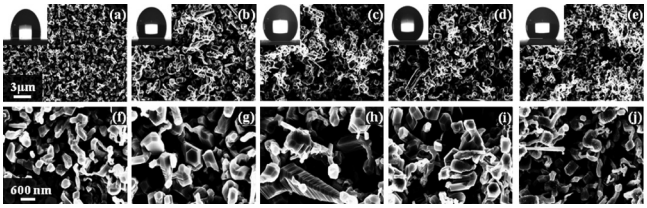

FIG. 2. FESEM images of Zn–ZnO coatings prepared at different thicknesses: (a) 1.8 μm, (b) 6.2 μm, (c) 8 μm, (d) 13 μm, and (e) 17 μm. The corresponding high resolution images are shown in (f)–(j). The insets show optical images of the corresponding CAs on the surface.

oxidation temperature, coating thickness, and sputtering power are shown in Fig. 1. It is to be noted that in a given set of experiments, a single parameter was varied keeping the other parameters constant. Further, the duration of thermal oxidation was maintained at 2 h regardless of the oxidation temperature. From Fig. 1, it can be seen that an oxygen flow rate of 75 SCCM, oxidation temperature of 300 °C, coating thickness of 13 μm and sputtering power of 85 W resulted in a CA greater than 150°. It is also observed that an increase in any of the parameters beyond the optimized value resulted in a CA value below 150°. Among all the process parameters, the coating thickness played a crucial role in determining the superhydrophobicity. Therefore, the coating thickness was optimized judiciously as it affects the microstructure of the Zn–ZnO coating significantly. Figures 2 and 3 show the plan view and cross-section FESEM images of coatings of different thicknesses. The insets in Fig. 2 show the corresponding CA images of the coatings. The 1.8 μm thick coating [Figs. 2(a) and 3(a)] has a somewhat orderly nanorodlike microstructure which becomes highly disordered as the coating thickness is increased. The 13 μm coating [Figs. 2(d) and 3(d)] has a nanoclusterlike microstructure rather than a nanorodlike microstructure. This coating exhibited a maximum CA of 154° and further increase in the coating thickness resulted in a decrease in the CA, possibly due to change in the surface roughness as will be discussed later. For all subsequent experiments, the coatings were prepared under optimized process conditions as described above.

In order to determine the effect of surface morphology on the wettability of Zn–ZnO surface, a coating prepared under optimized conditions was carefully studied using FESEM. The FESEM images are shown in Figs. 4(a)–4(d) at different magnifications. The low magnification FESEM image [Fig. 4(a)] shows a very smooth surface morphology. However, the high resolution images [Figs. 4(b) and 4(c)] show the presence of solid components (i.e., whitish regions)

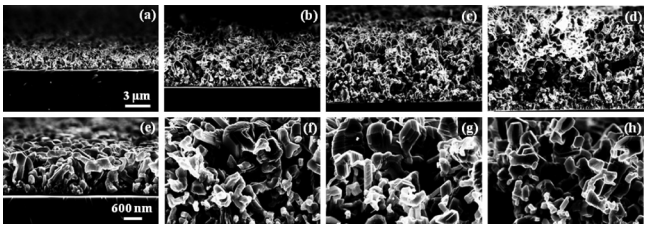

FIG. 3. Cross-sectional FESEM images of Zn–ZnO coatings prepared at different thicknesses: (a) 1.8 μm, (b) 6.2 μm, (c) 8 μm, and (d) 13 μm. The corresponding high resolution images are shown in (e)–(h).

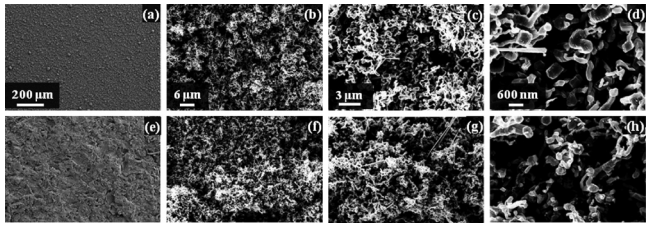

FIG. 4. FESEM images of Zn–ZnO coating prepared on plain glass substrate taken at different magnifications [(a)–(d)]. The corresponding FESEM images of Zn–ZnO coating deposited on a sand blasted glass substrate (R_a =4.5 μm) are shown in (e)–(h).

and air pockets (i.e., darker regions). This combination of air gaps and solid regions behaves as the first or higher scale roughness of the coating as shown in roughness profile data obtained from a profilometer [Fig. 5(a)]. The average roughness of this sample was in the nanometric scale (approximately 225 nm). Examination of the samples under very high magnification [Fig. 4(d)] showed the solid surface to consist of fused individual structures which generated a textured or a patterned surface. The textured surface acts as the second or lower scale roughness (believed to be few tens of nanometers). This texturing gives rise to a multiscale roughness in the Zn–ZnO coating which was responsible for the observed superhydrophobicity. To study the effect of an additional micron-scale roughness on the wettability of the Zn–ZnO coating, the glass substrates were sand blasted with 40 μm grit size alumina to generate a surface roughness of 4.5 μm [Fig. 5(b)]. The FESEM images of the sample with the additional micron-scale roughness are shown in Figs. 4(e)–4(h). Figure 4(e) shows the low resolution image of the surface, exhibiting a fractal like microstructure. High reso-

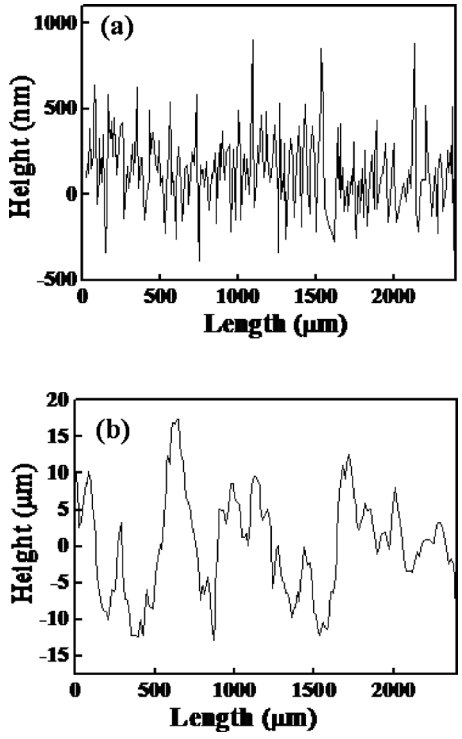

FIG. 5. Roughness profiles of Zn–ZnO coatings prepared on: (a) plain glass and (b) sand blasted glass substrates.

Author complimentary copy. Redistribution subject to AIP license or copyright, see http://jap.aip.org/jap/copyright.jsp

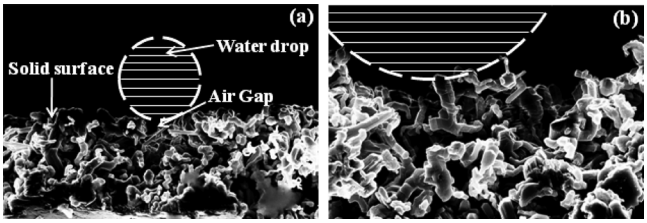

FIG. 6. Schematic of the behavior of a water droplet on a nanometric multiscale rough coating. The air gaps and solid surfaces are clearly shown in (a) and (b).

lution images of the coating [Figs. 4(f)–4(h)] show that the surface consisting of the solid regions and air gaps is similar to that of Zn–ZnO deposited on a smooth glass substrate. This surface consists of a micron-scale roughness in addition to a nanometric multiscale roughness. It was observed that the introduction of an additional micron-scale roughness resulted in a negligible change in the CA of the coating (CA =155°, cf. 154° for untreated glass). These results conclusively demonstrate that Zn–ZnO surfaces exhibit superhydrophobicity with only nanometric multiscale roughness, without the necessity of an additional micron-scale roughness as has been reported for other superhydrophobic surfaces.

The schematic representation of a water droplet on a nanometric multiscale rough Zn–ZnO coating is shown in Fig. 6. It can be seen from Figs. 6(a) and 6(b) that the water droplet balances on the solid surface bridging the air gaps giving rise to a high CA. As will be discussed later, an optimum ratio of solid surface and air gaps is necessary for superhydrophobicity.

The optimized Zn–ZnO coatings were characterized using XRD and XPS. Figure 7(a) shows the XRD pattern of thermally oxidized Zn–ZnO coating. The peaks centered at 2θ=31.9° and 36.3° correspond to (100) and (101) planes, respectively, of hexagonal-wurtzite ZnO. The peaks observed at 2θ=36.3°, 39.0°, 43.2°, and 54.3° correspond to the (002), (100), (101), and (102) planes, respectively, of metallic hexagonal Zn. The presence of diffraction peaks from both Zn and ZnO indicate that only the surface layer of the coating has been oxidized. Figures 7(b) and 7(c) show the Zn $2p_{3/2}$ and O 1*s* XPS core level spectra of the Zn–ZnO sample. The deconvolution of the Zn 2*p* peak indicated that it comprised of two peaks, centered at 1021.1 and 1021.8 eV. These can be attributed to the presence of zinc in the oxide and metallic

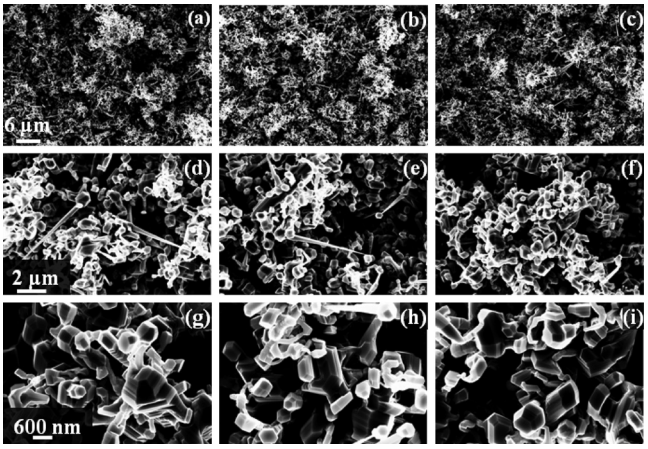

FIG. 8. FESEM images of Zn–ZnO coating taken at different time intervals: (a) immediately after deposition, (b) 24 h after the deposition, and (c) six days after the deposition. The corresponding high resolution images are shown in (d)–(i).

form, respectively.[20,21] The deconvolution of the O 1*s* peak resulted in two peaks centered at 530.8 and 532.9 eV. These correspond to the O^{2-} ion in the wurtzite structure of hexagonal Zn^{2+} ion array and to the oxygen deficient regions in the ZnO matrix.[22]

B. Self-diffusion of zinc

It was observed that the Zn–ZnO coatings demonstrated superhydrophobic properties 24 h after the deposition was completed. The CA measured immediately after the deposition was found to be approximately 127° which increased to approximately 154° when the coating was left in ambient conditions for 24 h. In order to provide a suitable explanation for the above observations, the coatings were studied carefully during this period using FESEM and micro-Raman spectroscopy. Soon after the samples were removed from the deposition chamber, AFM images of the coatings were also recorded. Figure 8 shows the FESEM images, at different magnifications, of the optimized coating with time. Figures 8(a), 8(d), and 8(g) are those of the coating taken soon after the deposition process, Figs. 8(b), 8(e), and 8(h) were taken 24 h later and Figs. 8(c), 8(f), and 8(i) were taken six days after the deposition process. The coating was kept in ambient conditions in between the successive measurements. Comparing the low resolution images in Figs. 8(a) and 8(b), it can be seen that the fraction of the solid components (whitish

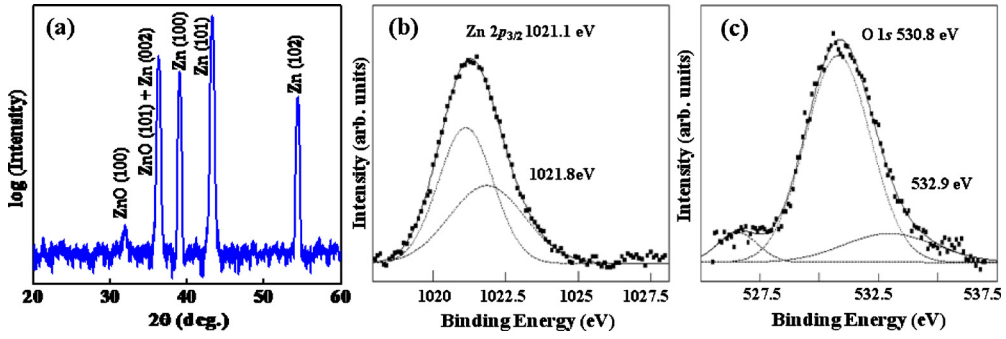

FIG. 7. (Color online) (a) XRD plot of an optimized coating, (b) and (c) XPS plots of Zn 2*p* and O 1*s* spectra.

Author complimentary copy. Redistribution subject to AIP license or copyright, see http://jap.aip.org/jap/copyright.jsp

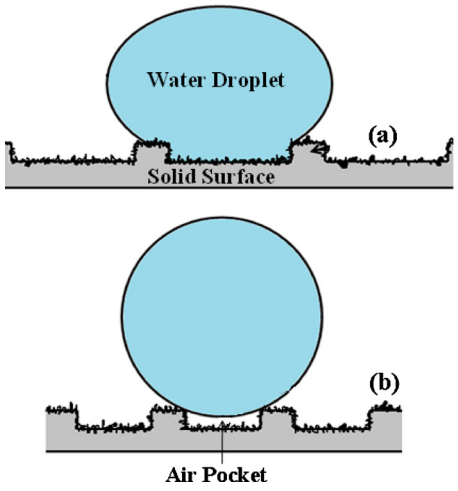

FIG. 9. (Color online) A schematic representation of a water droplet on a solid surface with different ratios of solid to air pockets.

regions) increases and that of the air pockets (darker regions) reduces. The fraction of the solid components after 24 h is almost similar six days later [Figs. 8(c), 8(f), and 8(i)]. Immediately after deposition, the fraction and size of the air pockets in the Zn–ZnO coating is high. Under this condition, part of a water droplet placed on the surface sinks into the air pockets and as a result, the surface does not demonstrate superhydrophobicity. As the fraction of the solid component increases, the surface composition reaches an ideal value wherein a droplet placed on the surface balances on the solid surface bridging the air pockets thereby giving rise to the superhydrophobic nature of the coating. This observation is schematically shown in Fig. 9. The multiscale nanometric rough nature of the coating is also depicted in the schematic diagram. The higher scale roughness is due to the protrusions or postlike microstructure while the lower scale of roughness is caused by the roughness on the surface of the post. From Figs. 9(a) and 9(b) it is clearly seen that a reduction in the air pockets and an increase in the fraction of the solid regions cause an increase in the CA.

To validate the above observations, we measured the roughness of the Zn–ZnO coatings as a function of time. The roughness profiles of the coatings taken at different time intervals are plotted in Fig. 10. Figures 10(a)–10(c) show the roughness profile taken 3 h, 22 h, and 49 h after the deposition process, respectively. It was observed that the roughness of the sample reduced with time. The average roughness values at 3 h, 22 h, and 49 h are 251 nm, 229 nm, and 218 nm, respectively. The reduction in the roughness values is consistent with the observations recorded using FESEM images. As the density of the solid component increases, the roughness of the coating reduces. These results were further corroborated using AFM, wherein measurements were recorded at the same spatial location on the coating as a function of time and drifts due to thermal expansion were corrected accordingly. For these measurements, a Zn–ZnO coating of approximately 2.0 μm thickness was used because of the instrument limitations. The AFM images of the coating taken soon after deposition are shown in Fig. 11. Figure 11(a) was taken approximately 10 min after the sample was removed

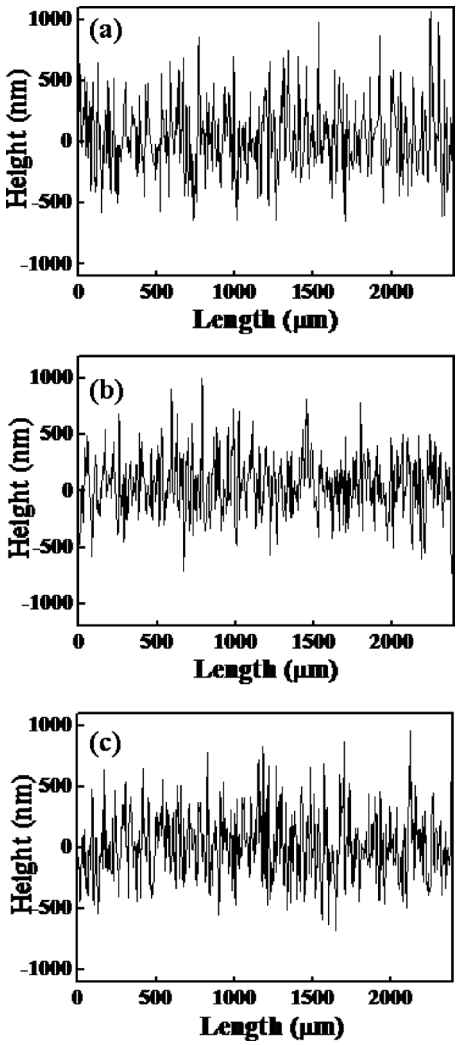

FIG. 10. Roughness profiles of a Zn–ZnO coating taken: (a) 3, (b) 22, and (c) 49 h after deposition. Corresponding values of roughness are 251 nm, 229 nm, and 218 nm, respectively.

from the deposition chamber and Fig. 11(b) was taken an hour later. It was observed that some individual peaks in Fig. 11(a) have fused together in Fig. 11(b) and vice versa. Two such locations have been highlighted with arrows in the figures. The above observations can be explained based on the phenomenon of outward self-diffusion of zinc to the surface of the coating and subsequent oxidation. At the time of thermal oxidation during the deposition, it is believed that only the top surface of the deposited Zn is converted to ZnO,

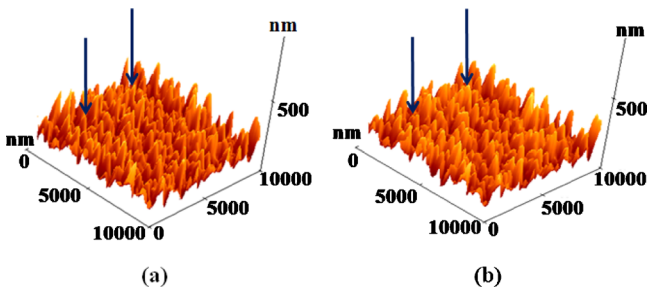

FIG. 11. (Color online) AFM images of a 2.0 μm thick Zn–ZnO coating recorded: (a) approximately 10 min after deposition and (b) 1 h later.

Author complimentary copy. Redistribution subject to AIP license or copyright, see http://jap.aip.org/jap/copyright.jsp

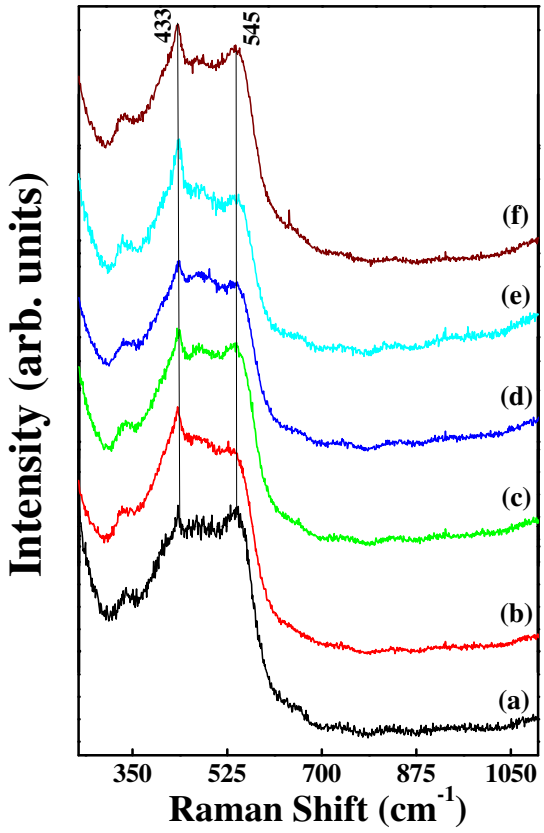

FIG. 12. (Color online) Micro-Raman spectra of Zn–ZnO coating recorded: (a) immediately, (b) 10, (c) 40, (d) 80, (e) 100, and (f) 3000 min after the deposition.

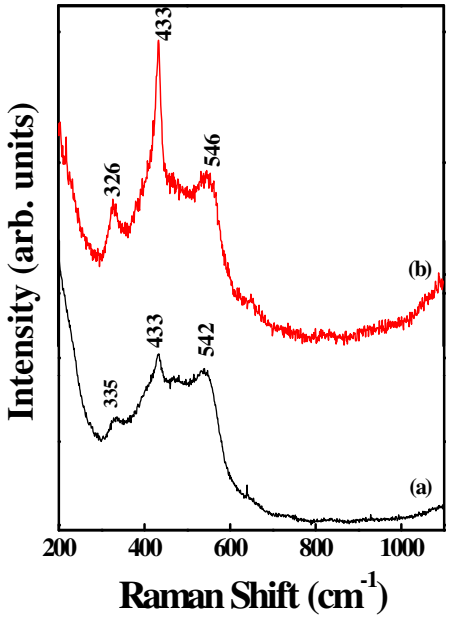

FIG. 13. (Color online) Micro-Raman spectra of: (a) as-deposited Zn–ZnO sample and (b) Zn–ZnO sample annealed at 350 °C in air for 2 h.

which is a few nanometers thick. This is because the rate of formation of ZnO, which is high initially, drops with time when the oxide layer reaches a certain thickness.[19] The reduction in the oxidation rate is observed in the low temperature oxidation of a number of metals.[23] Oxygen is initially adsorbed onto the surface of the metal oxide layer. Electrons tunnel through the oxide layer creating an electric field leading to a reduction in the activation energy of diffusion of metal ions through the oxide layer. The lower activation energy assists in the diffusion of metal ions to the surface of the oxide layer.[24–27] The diffused metal ions on the surface are subsequently oxidized, thereby increasing the thickness of the oxide layer. The process of metal ion diffusion ceases when the oxide layer reaches a certain thickness. Further diffusion occurs only under high temperatures.

To verify the hypothesis of outward self-diffusion of Zn in Zn–ZnO coatings, micro-Raman spectra of a coating were recorded with time (Fig. 12). The spectra were recorded at the same location on the surface of the coating. Figure 12(a) was recorded immediately after the sample was removed from the deposition chamber, Figs. 12(b)–12(f) were recorded 10, 40, 80, 100, and 3000 min after the deposition. The peak centered at 433 cm^{-1} is attributed to the E_2 (high) mode of ZnO and the peak at 545 cm^{-1} is attributed to oxygen deficient ZnO.[28,29] It is seen that the intensity of the two peaks fluctuates with time, alternately increasing and decreasing and finally reaching stability. The intensity of the E_2 (high) peak initially increases because the Zn present on the surface of the coating oxidizes, increasing the concentration of ZnO on the surface. This oxide layer consists of ZnO formed during the thermal oxidation in the deposition chamber and ZnO formed due to reaction of Zn with atmospheric oxygen. Due to the outward diffusion of Zn, the concentration of ZnO on the surface reduces and an increase in the intensity of the oxygen deficiency peak with a corresponding decrease in the E_2 (high) peak is seen. This Zn then reacts with the adsorbed oxygen resulting in an increase in the concentration of ZnO on the surface. The process of outward diffusion of Zn and subsequent oxidation due to reaction with atmospheric oxygen continues till a certain thickness of the oxide layer is reached. Beyond this, the rate of outward diffusion of Zn is very low and the coating stabilizes. The Raman spectra taken after extended duration (>3000 min) did not show any significant changes in the relative intensities of E_2 (high) mode and oxygen deficient ZnO peaks [Fig. 12(f)], suggesting the formation of a stable Zn–ZnO composition resulting in superhydrophobicity as discussed earlier.

Further, a sample of Zn–ZnO coating on silicon substrate was annealed in air at 350 °C. Micro-Raman spectrum of this sample was recorded after annealing and compared with the as-deposited sample [Fig. 13]. When the sample is annealed in air at 350 °C, further outward diffusion of Zn to the surface is expected to take place because of low activation of energy of diffusion. The diffused Zn reacts with the atmospheric oxygen giving rise to a higher concentration of ZnO in the coating. The oxidation of the diffused zinc increases the thickness of the oxide layer. This is seen in the very high intensity of the E_2 (high) peak of the sample annealed at 350 °C. It was observed that the sample annealed at 350 °C had different morphology as compared to the nonannealed sample thus affecting the wettability of the coating. The CA of the annealed sample was measured to be 78°. Figure 14 shows the FESEM images of the sample annealed at 350 °C. The low resolution image in Fig. 14(a) shows that the sample morphology resembles grains and grain bound-

Author complimentary copy. Redistribution subject to AIP license or copyright, see http://jap.aip.org/jap/copyright.jsp

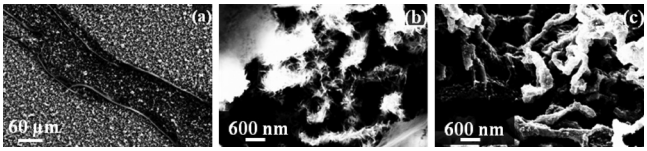

FIG. 14. FESEM images of a Zn–ZnO sample annealed at 350 °C: (a) low resolution image showing grain and grain boundarylike microstructure, (b) high resolution image from the grain boundary, and (c) high resolution image from the grain region.

aries. Figure 14(b) shows the high resolution image of the grain boundaries. It is seen that the morphology in the boundary regions consists of fiberlike microstructure. The high resolution image of the grain regions is shown in Fig. 14(c), which consists of microstructure similar to that seen in a typical Zn–ZnO coating but with nodal formation on the faces of the microstructure. This change in the morphology of the structure is responsible for the hydrophilic nature of the annealed Zn–ZnO coating in air.

In summary, the phenomenon of outward self-diffusion and subsequent oxidation of Zn causes morphological changes on the Zn–ZnO coating surface. The process of diffusion and oxidation of Zn takes place during the initial 24 h after deposition, thus affecting the CA significantly during this period. The microstructure of the Zn–ZnO coating subsequently gets stabilized, leading to a CA greater than 150°.

C. Effect of UV irradiation

The Zn–ZnO coatings were exposed to UV radiation under a 200 W lamp and the CAs were recorded. The coating was treated to UV radiation for 30 min at a time, with a period of an hour between successive treatments. It is to be emphasized here that the UV radiation did not generate any heat nor increase the temperature of the coating. It was observed that the CA reduced with the increasing time of exposure until it reached a stable value of approximately 60° after 4 h. The UV exposed samples were examined using FESEM and micro-Raman spectroscopy. Figure 15 shows the FESEM images of the coating before and immediately after a 60 min UV exposure. Figures 15(a), 15(c), and 15(e)

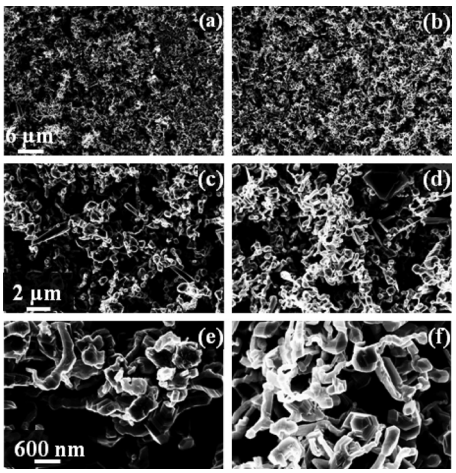

FIG. 15. FESEM images of Zn–ZnO coatings: (a) nonexposed sample and (b) UV exposed sample. The corresponding high resolution images are shown in (c)–(f).

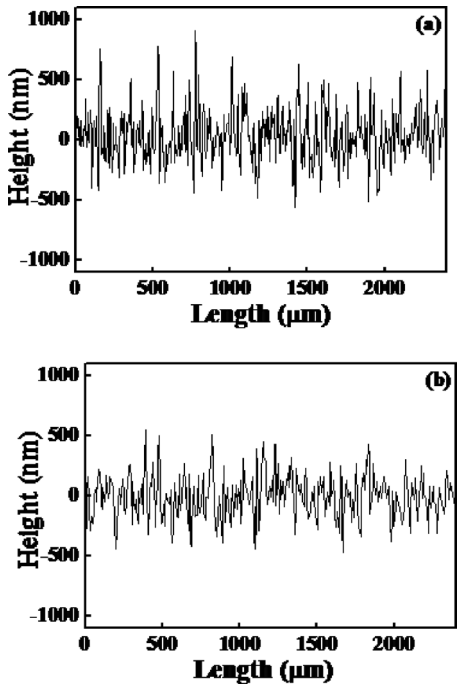

FIG. 16. Roughness profiles of: (a) nonexposed half and (b) UV exposed half of the same Zn- ZnO coating.

are FESEM images of the coating before the UV treatment. A comparison between Figs. 15(a) and 15(b) clearly shows that the density of the whitish portions, which are the Zn–ZnO nanoclusters, has increased and the air gaps (the darker regions in the image) has reduced. Therefore, a water droplet placed on the coating is in contact with a comparatively higher fraction of the solid surface than air gaps which results in a lower CA with water. We used the Cassie–Baxter equation to explain how an increase in the solid fraction causes a reduction in the CA of a surface:[30]

$$\cos\,\theta_{app} = f_1 \cos\,\theta_1 + f_2 \cos\,\theta_2,$$

where θ_{app} is the apparent CA on the composite surface, θ_1 and θ_2 are the CAs on the flat surface of components 1 and 2, respectively and f_1 and f_2 are the surface area fractions of the components 1 and 2, respectively. In our case, component 2 is air and the corresponding CA is 180°. As a result, the above equation is modified to:

$$\cos\,\theta_{app} = f_1(\cos\,\theta_1 + 1) - 1,$$

where component 1 is the Zn–ZnO coating. It can be clearly seen that as the value of f_1 increases, the corresponding value of θ_{app} decreases.

As can be seen from Fig. 15, UV exposure affects the surface morphology. From our earlier discussion, roughness profiles of a surface can be used to verify the morphological changes recorded using FESEM. For this, one half of an optimized sample was exposed to UV radiation for a period of 30 min. The roughness profiles of the nonexposed and UV exposed halves are shown in Fig. 16. The corresponding roughness values were approximately 189 nm and 157 nm, respectively. It was found that the roughness of the UV exposed region was considerably lower than the nonexposed region. The reduction in air gaps in the coating, which was

Author complimentary copy. Redistribution subject to AIP license or copyright, see http://jap.aip.org/jap/copyright.jsp

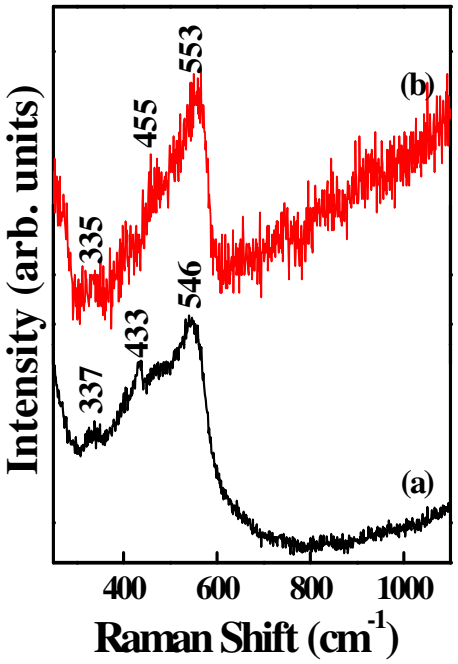

FIG. 17. (Color online) Micro-Raman spectra of: (a) nonexposed and (b) UV exposed Zn–ZnO coating.

observed in the FESEM images, is expected to lower the roughness of the coating. Furthermore, in order to study the chemical changes as a result of UV exposure, the samples were characterized using micro-Raman spectroscopy and the corresponding data is shown in Fig. 17. As has been discussed earlier, the nonexposed sample exhibited E_2 (high) and oxygen deficient ZnO peaks centered at 433 cm^{-1} and 546 cm^{-1}, respectively.[28,29] The micro-Raman spectra of the UV exposed sample when compared to that of the nonexposed sample exhibited an increase in the intensity of the peak attributed to oxygen deficiency. This is because the UV radiation creates electron–hole pairs. Some of the holes then react with the lattice oxygen which generate surface oxygen vacancies:[14,16]

$$ZnO + 2h\nu \rightarrow 2h^+ + 2e^-,$$

$$O^{2-} + h^+ \rightarrow O_1^- \quad \text{(surface trapped hole)},$$

$$O_1^- + h^+ \rightarrow 1/2O_2 + \square \quad \text{(oxygen vacancy)},$$

where h^+, e^-, and $\square$ represent a hole, an electron, and an oxygen vacancy. Water molecules may be dissociatively adsorbed onto the surface by coordinating into the oxygen vacancies. This causes a reduction in the CA of the surface with water. Also, the intensity of the E_2 (high) peak at 433 cm^{-1} after UV exposure is negligible when compared to the nonexposed sample which indicates the absence of ZnO on the surface. Upon UV illumination, oxygen vacancies are created leaving a very high concentration of Zn on the surface which leads to the reduction in the intensity of the E_2 (high) peak. It may also be possible that the outward diffusion of Zn is caused due to the vacancies created by the loss of oxygen from the surface, leading to microstructural changes as seen in FESEM data (Fig. 15). These results were further corroborated using AFM data. Figure 18 shows a comparison of the

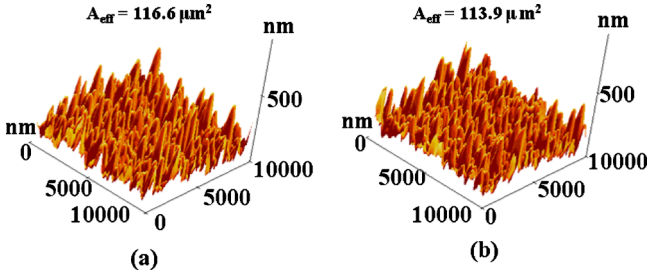

FIG. 18. (Color online) AFM images of a thin Zn–ZnO coating: (a) before UV exposure and (b) immediately after 30 min UV exposure.

typical AFM images of an approximately 2.0 μm thick Zn–ZnO coating before UV exposure and immediately after a 30 min UV exposure. The measurements were taken on a base area of 100 μm^2. It was observed that the actual surface area (A_{eff}) of the coating reduced after UV exposure. The surface area before exposure was around 116.6 μm^2 which dropped to around 113.9 μm^2 after the UV treatment. This supports the observations that the density of the air gaps reduced after UV treatment causing the overall area of the surface to reduce, resulting in a change in the CA.

IV. CONCLUSIONS

Zn–ZnO coatings prepared on glass substrates under optimum deposition conditions exhibited water CA > 150°. The CA attained a maximum value of 154° for a coating thickness of 13 μm and further increase in the coating thickness led to a loss of superhydrophobicity. This was attributed to: (i) an optimum density of solid regions (nanoclusters) and air pockets and (ii) presence of the hierarchical nanometric multiscale roughness. These coatings exhibited an average roughness (R_a) in the range 200–300 nm. Coatings deposited on sand blasted glass (R_a=4.5 μm) demonstrated similar wettability (CA=155°) as coatings deposited on plain glass substrates (CA=154°). A significant change in the CA of Zn–ZnO coatings was observed during the initial 24 h after deposition (approximately 125° to >150°). The corresponding changes in the microstructure of the coatings were observed under FESEM during this period. The FESEM data showed an increase in the density of the solid regions which attained stability 24 h later. The changes in the morphology were due to the outward self-diffusion and subsequent oxidation of Zn under ambient conditions. These observations were supported by the changes observed in the intensities of the E_2 (high) (433 cm^{-1}) and oxygen deficient (545 cm^{-1}) ZnO peaks. The annealing of Zn–ZnO coatings at 350 °C for 2 h in air caused an increase in the intensity of the E_2 (high) peak but a loss of superhydrophobicity (CA=78°). This was due to the formation of a completely different microstructure in the annealed sample compared to as-deposited Zn–ZnO sample. Furthermore, a change from superhydrophobic to hydrophilic nature was observed when the Zn–ZnO coatings were exposed to UV irradiation for short durations. The UV irradiation disturbed the densities of the solid regions (nanoclusters) and air pockets. These observations have been supported by a reduction in the roughness values after UV irradiation (189 to 157 nm) and a decrease in the effective

Author complimentary copy. Redistribution subject to AIP license or copyright, see http://jap.aip.org/jap/copyright.jsp

surface area (116.6 to 113.9 μm^2) as determined using AFM (measured on a base area of 100 μm^2). The UV irradiation of Zn–ZnO coatings also causes oxygen vacancies to be created on the surface of the coating and this was supported by micro-Raman data [i.e., loss of E_2 (high) peak and an increase in the intensity of oxygen deficient ZnO peak].

ACKNOWLEDGMENTS

The authors thank Director, NAL (CSIR) for giving permission to publish these results. Work presented in the manuscript is partially supported by CSIR under Grant No. FAC-00-01-11. Mr. N. Selvakumar, Mr. Siju, Mr. Praveen Kumar, and Mr. N. T. Manikandanath are thanked for the CA, FESEM, roughness profile, and micro-Raman measurements.

[1]C. Neinhuis and W. Barthlott, Ann. Bot. (London) **79**, 667 (1997).
[2]W. Barthlott and C. Neinhuis, Planta **202**, 1 (1997).
[3]W. Lee, M. K. Jin, W. C. Yoo, and J. K. Lee, Langmuir **20**, 7665 (2004).
[4]L. Feng, S. Li, Y. Li, H. Li, L. Zhang, J. Zhai, Y. Song, B. Liu, L. Jiang, and D. Zhu, Adv. Mater. **14**, 1857 (2002).
[5]T. Onda, S. Shibuichi, S. Satoh, and K. Tsujii, Langmuir **12**, 2125 (1996).
[6]A. Nakajima, A. Fujishima, K. Hashimoto, and T. Watanabe, Adv. Mater. **11**, 1365 (1999).
[7]W. Chen, A. Y. Fadeev, M. C. Heieh, D. Öner, J. Youngblood, and T. J. McCarthy, Langmuir **15**, 3395 (1999).
[8]Y. Wu, H. Sugimura, Y. Inoue, and O. Takai, Chem. Vap. Deposition **8**, 47 (2002).
[9]J. Genzer and K. Efimenko, Biofouling **22**, 339 (2006).
[10]A. Marmur, Biofouling **22**, 107 (2006).
[11]T. Kako, A. Nakajima, H. Irie, Z. Kato, Z. K. Uematsu, T. Watanabe, and K. Hashimoto, J. Mater. Sci. **39**, 547 (2004).
[12]D. Quéré, Rep. Prog. Phys. **68**, 2495 (2005).
[13]A. Duparré, M. Flemming, J. Steinert, and K. Reihs, Appl. Opt. **41**, 3294 (2002).
[14]X. Feng, L. Feng, M. Jin, J. Zhai, L. Jiang, and D. Zhu, J. Am. Chem. Soc. **126**, 62 (2004).
[15]Y. Liu, T. Tan, B. Wang, X. Song, E. Li, H. Wang, and H. Yan, J. Appl. Phys. **103**, 056104 (2008).
[16]H. Liu, L. Feng, J. Zhai, L. Jiang, and D. Zhu, Langmuir **20**, 5659 (2004).
[17]N. J. Shirtcliffe, G. McHale, M. I. Newton, G. Chabrol, and C. C. Perry, Adv. Mater. **16**, 1929 (2004).
[18]M. Nosonovsky, Langmuir **23**, 3157 (2007).
[19]R. Nakamura, J.-G. Lee, D. Tokozakura, H. Mori, and H. Nakajima, Mater. Lett. **61**, 1060 (2007).
[20]M. N. Islam, T. B. Ghosh, K. L. Chopra, and H. N. Acharya, Thin Solid Films **280**, 20 (1996).
[21]M. Chen, X. Wang, Y. H. Yu, Z. L. Pei, X. D. Bai, C. Sun, R. F. Huang, and L. S. Wen, Appl. Surf. Sci. **158**, 134 (2000).
[22]K. G. Saw, K. Ibrahim, Y. T. Lim, and M. K. Chai, Thin Solid Films **515**, 2879 (2007).
[23]N. Cabrera and N. F. Mott, Rep. Prog. Phys. **12**, 163 (1949).
[24]N. F. Mott, Trans. Faraday Soc. **35**, 1175 (1939).
[25]N. F. Mott, Trans. Faraday Soc. **36**, 472 (1940).
[26]N. F. Mott, Trans. Faraday Soc. **43**, 429 (1947).
[27]N. Cabrera, Philos. Mag. **40**, 175 (1949).
[28]M. Tzolov, N. Tzenov, D. Dimova-Malinovska, C. Pizzuto, G. Vitali, G. Zollo, and I. Ivanov, Thin Solid Films **379**, 28 (2000).
[29]X. L. Xu, S. P. Lau, J. S. Chen, G. Y. Chen, and B. K. Tay, J. Cryst. Growth **223**, 201 (2001).
[30]A. B. D. Cassie and S. Baxter, Trans. Faraday Soc. **40**, 546 (1944).

Author complimentary copy. Redistribution subject to AIP license or copyright, see http://jap.aip.org/jap/copyright.jsp